Laser-induced fluorescence characterization of ions in a magnetron plasma

M. J. Goeckner, J. Goree, and T. E. Sheridan
Department of Physics and Astronomy, The University of Iowa, Iowa City, Iowa 52242

(Received 19 January 1990; accepted 23 June 1990)

We report for the first time laser-induced fluorescence measurements of a sputtering magnetron plasma. From these measurements we determined the density, average velocity, and temperature of the ions. The ion density profile is peaked at the same location as the electron density profile, which was measured with a Langmuir probe. The average ion velocity parallel to the cathode surface is less than our detection limit of 93 m/s. The ions at the edge of the discharge are room temperature, while in the center of the discharge they reach a temperature of 0.64 eV. These temperatures are attributed to acceleration of the ions by the electric field in the plasma, together with collisional scattering.

I. INTRODUCTION

Sputtering magnetrons are used for thin film depositon and sputter etching.[1] These devices have an electric sheath and an external magnetic field configured to trap electrons.[2,3] Typically the magnetic field strength is weak enough that the electrons are magnetized, but the ions, due to their larger mass, are unmagnetized.[3] The ions are accelerated by the electric field in the sheath. Upon striking the cathode they sputter material from the surface[2,4] and cause secondary electron emission.[5]

Several experimenters have characterized magnetron plasmas. Rossnagel and Kaufman,[6] and Bell and Glocker[7] have determined the electron densities and temperatures in their magnetrons. Wendt[8] measured the radial profile of the ion current at the cathode surface. Using the same device, Gu and Lieberman[9] recorded the plasma glow intensity as a function of distance above the cathode. Rossnagel[10] reported a rarefaction of the neutral density, which he attributed to the sputtering wind. In a previous paper,[11] we demonstrated that the ion mass and the particle confinement time are linked.

In this paper we report for the first time laser-induced fluorescence (LIF) characterization of the ions in a sputtering magnetron discharge. The LIF technique has the advantages of being nonperturbing, *in situ*, and spatially resolved. In particular, we measured the ion velocity distribution function and from this we have calculated the ion density, the average ion velocity, and the ion temperature. These parameters are important because the ion flux and the ion energy at the cathode regulate the sputtering yield.[12]

In the next section, we describe the experiment in which we characterized the ions in the magnetron discharge. In Sec. III we present both LIF and Langmuir probe results, showing that the ion density is higher and that the ions are more energetic in the location of the electron trap. In Sec. IV we attribute the measured temperatures to acceleration of the ions by an electric field in the plasma, together with collisional scattering.

II. EXPERIMENT

The plasma was produced with a cylindrically symmetric planar dc magnetron, which has been described in detail elsewhere.[13] On the copper cathode surface ($z = 0$) the magnetic field is entirely radial at $r = 1.7$ cm and has a magnitude of 245 G. Here z is the height above the cathode surface and r is the distance from the symmetry axis. The magnetic field is almost cylindrically symmetric, with an azimuthal rms variation of only 2.6%. We operated the plasma with a voltage regulated cathode bias of -400 V and an argon gas pressure of 0.96 Pa, resulting in a discharge current of 150 mA. Under these conditions, the electron confinement time and the ion transit time $\tau_{\rm trans}$ were reported to range from 0.6 to 0.9 μs,[13] while the sheath thickness is on the order of 1 mm.

Because the electron trap is localized,[3] the plasma is nonuniform. The location of the trap is revealed by Langmuir probe measurements of the electron temperature T_e, the electron density n_e, and the plasma potential V_p. (In this paper all temperatures are given in units of energy.) The radial profiles of T_e and n_e at $z = 1.03$ cm, shown in Fig. 1,

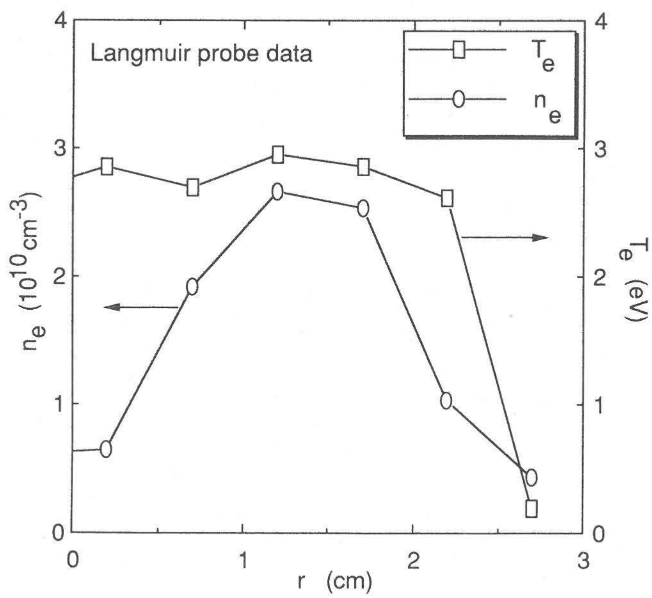

FIG. 1. Electron density n_e and temperature T_e as a function of the radial position r. These Langmuir probe measurements, taken at a height of 1.03 cm above the cathode surface, show that the electron trap is localized to 0.5 cm $< r <$ 2.0 cm.

and a map of V_p, shown in Fig. 2, indicate that the ring-shaped trap is near $r = 1.7$ cm.

We used LIF[14] to measure the time averaged velocity distribution function of the excited-state ions in the presheath region of the plasma. This was accomplished by tuning the laser through the 617.228 nm ArII spectral line from the $(^1D)3d\,^2G_{7/2}$ metastable state,[15] and sampling the intensity of the emitted fluorescence photons at 458.990 nm. To improve the signal-to-noise ratio, we averaged over 140 laser pulses for each wavelength of the laser. The laser excited to a higher state only those ions with a velocity satisfying the Doppler shift condition

$$2\pi\Delta\nu = \mathbf{v}\cdot\mathbf{k} = v_{\parallel} k. \tag{1}$$

Here $\mathbf{k}$ is the incident laser photon wave vector, $\mathbf{v}$ is the ion velocity, $v_{\parallel}$ is the component of the ion velocity parallel to the direction of the laser beam, and $\Delta\nu$ is the difference between the laser frequency and the transition frequency of a stationary ion. Because of the dot product between $\mathbf{v}$ and $\mathbf{k}$, the LIF line shape corresponds to the shape of the velocity distribution projected along the direction of the laser beam, in other words the shape of the reduced distribution function $f_i^*(v_{\parallel})$. While the natural linewidth,[16] pressure broadening,[17] Stark broadening,[17,18] Stark splitting,[19] Zeeman splitting,[19] and instrumental broadening[20,21] may spoil an LIF measurement of $f_i^*(v_{\parallel})$, such distortions were negligible for this experiment. In the Appendix we argue that the distribution of the excited ions is similar to the distribution of the ions as a whole.

The layout of the optical systems, the plasma, the magnetron, and the coordinate system are sketched in Fig. 3. We used a pulsed tunable dye laser (Lumonics HD-SLM) which operated in a single longitudinal mode[22] with a Fourier-transform-limited bandwidth. The beam passed through the discharge parallel to the cathode surface at a height of 0.98 cm. The fluorescence from the plasma was collected by the detection optics, which were aligned to view in a direction orthogonal to both the beam path and the symmetry axis of the magnetron. The intensity of the LIF was detected by a photomultiplier tube, which we did not calibrate. As is shown in Fig. 4, the intersection of the viewing cone and the laser beam determined the probed region. This region was a cylinder, 1.0 cm in diameter and 0.84 cm long. It was localized to the plasma, i.e., presheath, region and did not include the sheath region. When we measured the azimuthal component of the velocity, the optics were aligned with the configuration of Fig. 4 so that the viewing cone intersected the symmetry axis. When we measured radial velocity component, on the other hand, the laser beam was aligned so that it intersected the symmetry axis. We also routed a portion of the laser beam through an iodine cell to calibrate the laser frequency against the molecular spectrum tabulated in an atlas.[23] The gated sampler simultaneously recorded the LIF signals from both the iodine cell and the plasma.

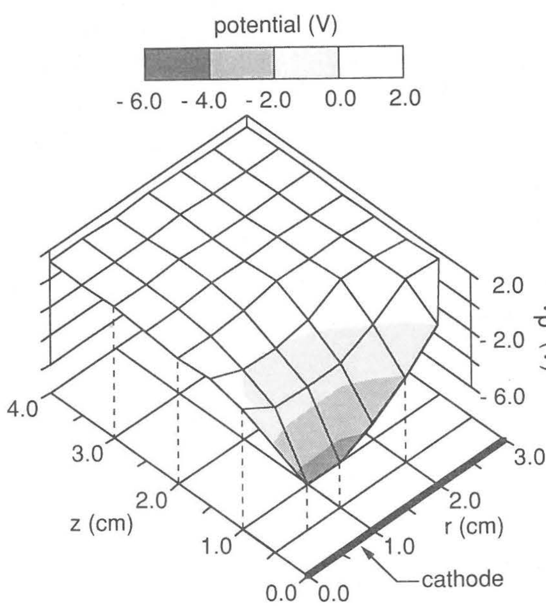

FIG. 2. Electric potential in the presheath as a function of the radial position r and the axial position z. These Langmuir probe measurements of the plasma potential V_p show that the potential drop is largest for 0.5 cm $< r <$ 2.0 cm. The ions fall down this electric potential toward the cathode.

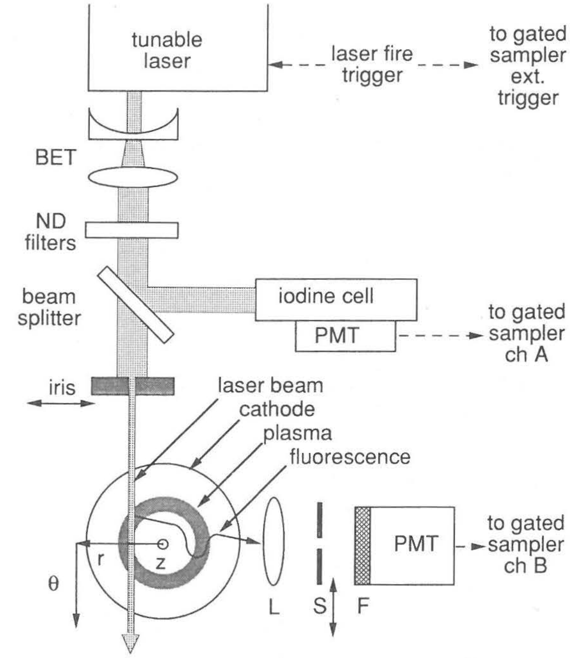

FIG. 3. Schematic of the experimental layout. The equipment shown includes a beam expanding telescope (BET), a set of removable neutral density (ND) filters, a movable iris, a 100 mm diameter lens (L), a 10% beam splitter, a movable 7 mm wide slit (S), a 9 nm bandpass interference filter (F), and two photomultiplier tubes (PMT). This figure also shows the r, θ, and z, coordinates, corresponding to the radial, azimuthal, and axial directions. The optical geometry near the cathode is shown in more detail in Fig. 4.

III. RESULTS

By scanning the laser frequency through the 617.228 nm ArII transition, we obtained a Doppler-broadened line shape, as shown in Fig. 5. This scan was used to characterize the reduced velocity distribution $f_i^*(v_{\parallel})$ by fitting a Maxwellian to the line shape. We chose to use a Maxwellian not

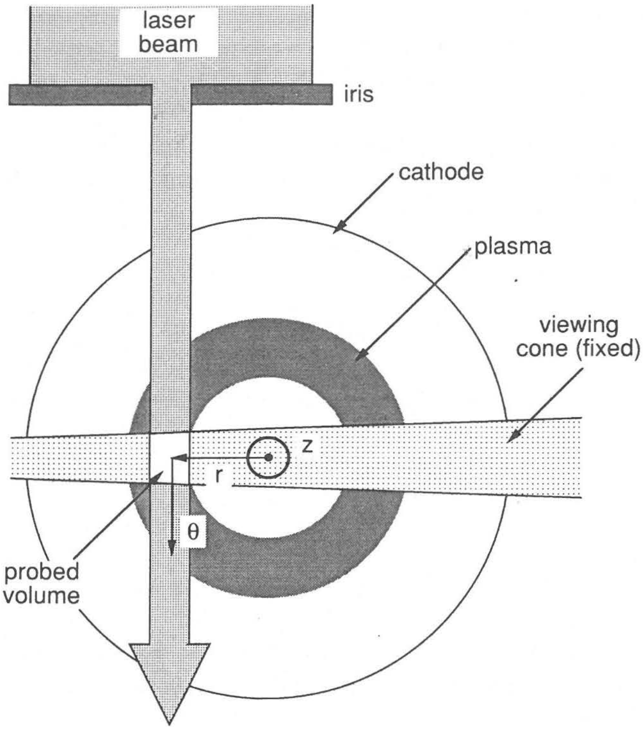

FIG. 4. Configuration for measuring the reduced distribution function of the excited-state ions $f_i^*(v_\parallel)$ along the azimuthal direction. We aligned the detection optics so that the viewing cone intersected the symmetry axis. The iris was movable to allow us to scan the radial position of the laser beam in the plasma. A similar configuration, not shown here, was used for measuring $f_i^*(v_\parallel)$ along the radial direction.

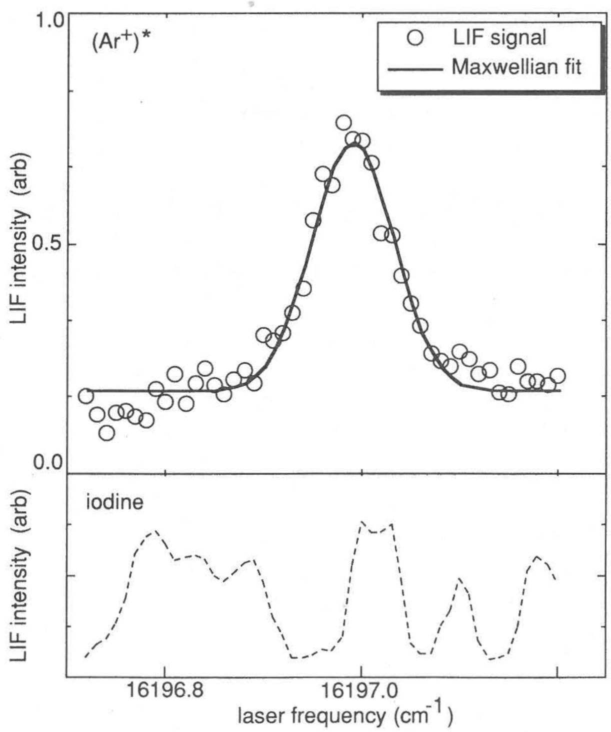

FIG. 5. LIF intensity as a function of the laser frequency. This line shape can be equated with the shape of $f_i^*(v_\parallel)$ along the direction of the laser beam. Also shown are a Maxwellian fit (Ref. 24) of $f_i^*(v_\parallel)$ and the simultaneously measured iodine spectrum. The iodine spectrum was used to calibrate the vacuum wave number of the laser.

because the ions are in thermal equilibrium, as indeed they are not,[24] but because it appears to offer a good fit, as demonstrated in Fig. 5. We also performed a scan of the 611.492 nm transition and the 612.336 nm transition to verify that the spectral line shapes were the same.

Using the 617.228 nm transition, we measured the azimuthal and radial velocity components as functions of the radial position. We never measured the axial component.

By integrating over the distribution, we determined the relative density of the metastable ions, $n_i^* = \int f_i^*(v_\parallel)dv_\parallel$. The resulting radial profile of n_i^* is shown in Fig. 6. The profile is peaked in the trap region at nearly the same radius as the electron density profile in Fig. 1.

The average ion velocity (i.e., the drift velocity) is given by the first moment of the distribution function, $\langle v_i^* \rangle = \int v_\parallel f_i^*(v_\parallel)dv_\parallel$. We found that the average ion velocity in the azimuthal and radial directions was less than our detection limit of 93 m/s. In the axial direction, which we did not measure, one would expect the ions to attain a much higher average velocity as they are accelerated toward the cathode.

The effective ion temperature[24] T_i^{eff}, which is proportional to the average ion energy [i.e., $T_i^{\text{eff}} \propto \int v_\parallel^2 f_i^*(v_\parallel)dv_\parallel$] ranges from room temperature to as high as 0.64 eV, as shown in the profiles in Fig. 7. The hottest ions are found near the center of the electron trap, while the coolest are located near the axis of symmetry, which is outside the trap. The azimuthal and radial velocity components do not have the same effective temperature. For the azimuthal direction, T_i^{eff} has a peak of 0.64 eV, while the ions are cooler for the radial direction, with a peak of 0.26 eV. These densities and effective temperatures are discussed in more detail in the next section.

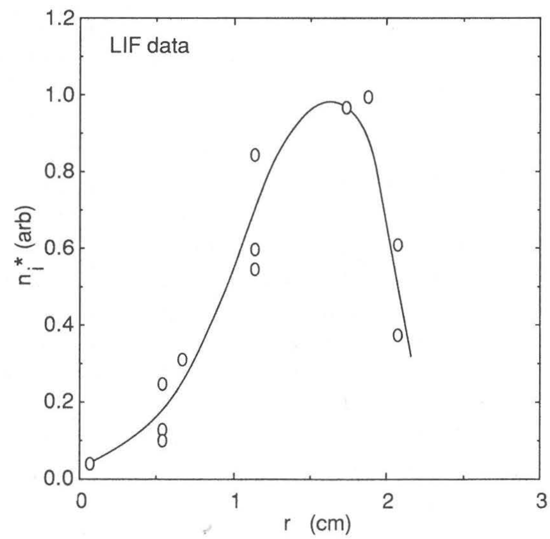

FIG. 6 Ion density n_i^* as a function of the radial position. We determined the ion density by integrating $n_i^* = \int f_i^*(v_\parallel)dv_\parallel$. The radial profile of n_i^* peaks at nearly the same location as the radial profile of n_e shown in Fig. 1. A line showing the general trend has been drawn through the data.

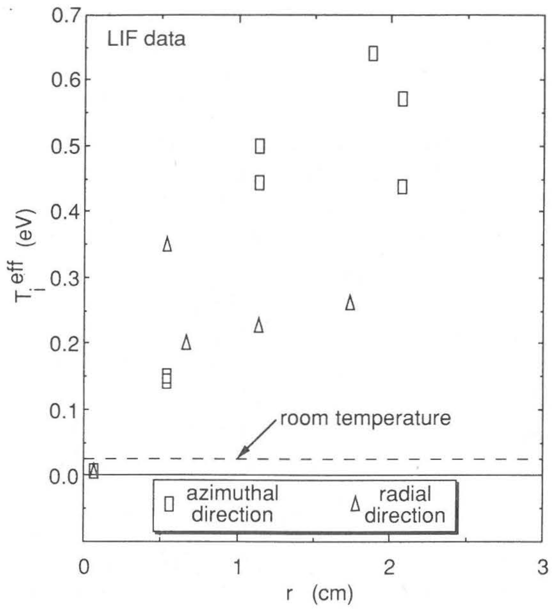

FIG. 7. Ion temperature $T_i^{\rm eff}$ in units of energy as a function of the radial position. The effective ion temperature was calculated from a Maxwellian fit of the velocity distribution. The azimuthal velocity component has a temperature of 0.64 eV in the center of the trap while the temperature of the radial component is only 0.26 eV.

IV. DISCUSSION

The ion densities and effective temperatures we measured must be accounted for by ion transport and the location of ionization events. Ionization predominately takes place in the trap region where the energetic electrons are localized. Ions are transported from their ionization sites by (1) acceleration by the dc electric field, usually toward the cathode, while possibly undergoing (2) collisions with neutrals or (3) scattering by a turbulent electric field. We examine these three processes below, and find that all three may contribute to the effective temperature.[25]

The first mechanism, falling down the dc potential hill, is significant because the ions are born at various locations and thus on different equipotentials. Ions at a given point in the plasma will have fallen over a range of different potential drops, thereby acquiring a distribution of velocities. The electric potential contours shown in Fig. 2 indicate that the potential energy varies by several eV over the trap region where the ions are produced. Therefore, this process could bring about a range of energies corresponding to an effective temperature as high as the ones we have measured in the radial direction. Coupled with the spatial distribution of the ionization events, this mechanism should also bring about ion density profiles that are peaked in the vicinity of the electron trap, as we found them to be in the experiment. We have tested these two conclusions quantitatively using a numerical simulation of the free fall process, to be reported in another paper.[25]

This free fall process, however, can result in a spread in velocities only in the radial and axial directions, because the potential has a gradient only in those directions. The potential cannot have a gradient in the azimuthal direction due to symmetry, and thus, there cannot be an electric field to influence the ion velocity in the azimuthal direction. Our experimental results show that there is a significant effective temperature for the azimuthal velocity component, indicating that an additional process must be occurring.

Ion–neutral collisions, the second mechanism, also partly determine the effective ion temperature. Both elastic and charge exchange collisions must be considered. Elastic scattering will broaden the distribution function, increasing the effective ion temperature, as we now demonstrate. The mean time $\tau_{\rm trans}$ that elapses between an ion's birth in the trap and its collection at the cathode was reported by Sheridan and Goree[13] to range from 0.6 to 0.9 μs. This can be compared to the rate of elastic collisions,[26] $\nu_{\rm el} \approx 4.3\times 10^5$ s^{-1} in our discharge. We find $\tau_{\rm trans}\nu_{\rm el} \approx 0.4$, indicating that an ion has a 40% chance of having an elastic collision during its transit to the cathode. At the time of the collision an ion in the presheath may have gained several eV of energy from falling down the potential hill. Thus, it is reasonable to expect that ions can acquire an effective temperature for the azimuthal direction as high as the 0.64 eV we have measured. This temperature is also consistent with the theoretical results of Kock and Huchon for a presheath with this degree of collisionality.[27]

Charge exchange collisions have approximately the same cross section as elastic collisions[26] and will tend to equilibrate the ion temperature with that of the more numerous neutral atoms. Because the neutral gas temperature is unknown, and is almost certainly not room temperature everywhere,[10] the contribution of charge exchange collisions to the ion temperature is uncertain. We speculate that the ion temperature is probably greater than the neutral temperature, and therefore charge exchange collisions will cool the ions.

One must also consider the third mechanism, low-frequency turbulence. Using a turbulent electric field of 0.4 V/cm for our magnetron, as reported in Ref. 13, we calculated that the ions can gain energy of order 0.4 eV from this field. Thus, our results might be due to measuring the time averaged distribution, which includes ions that were accelerated by different turbulent fields, and not the instantaneous distribution. Accordingly, we conclude that the free fall and collisional scattering processes are likely to lead to the effective ion temperatures we have measured. However, it is unclear why our effective temperature is higher in the azimuthal direction than in the radial direction.

IV. SUMMARY

We have reported the first LIF measurements of ion densities, average ion velocities, and effective ion temperatures in a sputtering magnetron discharge. The average ion velocities were below our detection limit of 93 m/s, while the radial profiles of n_i^* and $T_i^{\rm eff}$ were peaked in the center of the electron trap. The effective temperature for the azimuthal velocity component ranges from room temperature to 0.64 eV in the center of the trap, while the effective temperature for the radial component has a peak of 0.26 eV.

These results are qualitatively explained by assuming that ion-neutral collisions contribute to the dynamics of the ions as they are accelerated by the presheath electric field toward the cathode.

ACKNOWLEDGMENTS

This work was funded by a grant from the Iowa Department of Economic Development and an IBM Faculty Development Award.

APPENDIX: COMPARISON OF THE GROUND-STATE AND EXCITED-STATE IONS

Here we enumerate the collisions capable of producing $(Ar^{+})^{*}$ in a low-temperature discharge:

$$Ar + e^{-}_{energetic} \rightarrow (Ar^{+})^{*} + 2e^{-}, \quad (A1)$$

$$Ar^{+} + e^{-}_{energetic} \rightarrow (Ar^{+})^{*} + e^{-}, \quad (A2)$$

$$Ar^{+} + h\nu \rightarrow (Ar^{+})^{*}, \quad (A3)$$

$$Ar + h\nu \rightarrow (Ar^{+})^{*}, \quad (A4)$$

$$Ar^{+} + Ar \rightarrow (Ar^{+})^{*} + Ar, \quad (A5)$$

$$Ar^{+} + Ar \rightarrow Ar + (Ar^{+})^{*}, \quad (A6)$$

$$Ar^{+} + Ar^{+} \rightarrow (Ar^{+})^{*} + Ar^{+}, \quad (A7)$$

$$Ar^{+} + Ar^{+} \rightarrow (Ar^{+})^{*} + (Ar^{+})^{*}. \quad (A8)$$

For our discharge, reaction (A1) dominates the production of the $(Ar^{+})^{*}$ (see Table I). The rate of excitation of ground state ions by energetic electrons, reaction (A2), is much slower than the rate of reaction (A1). The photon processes (A3) and (A4) are not important because the plasma is optically thin. Reactions (A5)–(A8) do not take place because in the discharge the impact energies are less than the corresponding thresholds.

Finally, we must demonstrate the suitability of using measurements of ions in the excited state to characterize the ions as a whole. Because both the ground-state ions and the excited-state ions are predominantly produced by single-step electron-impact ionization, their velocity distributions will have the same shapes and spatial variations if the cross sections for creating these ion species are similar. Any discrepancy between the two distributions arises mainly from the difference in the threshold energies of the two cross sections (15.8 eV compared to 34.9 eV). Since the difference between these two thresholds is much less than the − 400 V cathode potential, we can conclude that our measurements are suitable for characterizing the ions as a whole, provided that the electrons born on the cathode are primarily responsible for sustaining the discharge.

TABLE I. Rate of production of $(Ar^{+})^{*}$. Reaction (A1) has the fastest rate, 2.29×10^{14} $cm^{-3}\,s^{-1}$. The rates listed below were computed assuming that: the neutral density is 2.69×10^{14} cm^{-3}, the ion density is 2.69×10^{10} cm^{-3}, the soft x-ray photon density is $<10^{6}$ cm^{-3}, and the impact energies are characterized by $T_i \approx T_n \approx 0.5$ eV. The value used for the soft x-ray density assumes that these photons carry away less than one thousandth of the power supplied to the magnetron.

Reaction	Rate of $(Ar^{+})^{*}$ production [relative to reaction (A1)]	Cross section Ref.
(A1)	1	28
(A2)	10^{-3}	29
(A3)	$<10^{-3}$	30
(A4)	$<10^{-3}$	31
(A5)	0	
(A6)	0	
(A7)	0	
(A8)	0	

[1] John A. Thornton and Alan S. Penford, in *Thin Film Processes*, edited by J. L. Vossen and W. Kern (Academic, New York, 1978), p. 75.

[2] Brian Chapman, *Glow Discharge Processes* (Wiley–Interscience, New York, 1980), pp. 177–184 and 265.

[3] T. E. Sheridan, M. J. Goeckner, and J. Goree, J. Vac. Sci. Technol. A **8**, 30 (1990).

[4] John A. Thornton, J. Vac. Sci. Technol. **15**, 171 (1978).

[5] Mark A. Lewis, David Glocker, and Jacob Jorne, J. Vac. Sci. Technol. A 7, 1019 (1989).

[6] S. M. Rossnagel and H. R. Kaufman, J. Vac. Sci. Technol. A **4**, 1822 (1986).

[7] Brent C. Bell and David Glocker, J. Vac. Sci. Technol. A **6**, 2047 (1988).

[8] A. E. Wendt, Ph.D. thesis, University of California at Berkeley, 1988; A. E. Wendt, M. A. Lieberman, and H. Meuth, J. Vac. Sci. Technol. A **6**, 1827 (1988).

[9] Lan Gu and M. A. Lieberman, J. Vac. Sci. Technol. A **6**, 2960 (1988).

[10] S. M. Rossnagel, J. Vac. Sci. Technol. A **6**, 19 (1988).

[11] T. E. Sheridan, M. J. Goeckner, and J. Goree, J. Vac. Sci. Technol. A **8**, 1623 (1990).

[12] J. Bohdansky, "Sputtering," in *Data Compendium for Plasma-Surface Interactions*, special issue 1984, Nucl. Fusion, 61-72 (1984).

[13] T. E. Sheridan and J. Goree, J. Vac. Sci. Technol. A **7**, 1014 (1989).

[14] R. A. Stern and J. A. Johnson III, Phys. Rev. Lett. **34**, 1548 (1975).

[15] Stanley Bashkin and John A. Stoner, Jr., *Atomic Energy Level & Grotrian Diagrams* 2 (North–Holland, New York, 1978), pp. 192–229.

[16] Gustavo García and José Campos, J. Quant. Spectrosc. Radiat. Transfer **34**, 85 (1985).

[17] Hans R. Griem, *Spectral Line Broadening by Plasmas* (Academic, New York, 1974), p. 32.

[18] Kenro Miyamoto, *Plasma Physics for Nuclear Fusion* (MIT, Cambridge, 1989), pp. 497–500.

[19] B. H. Bransden and C. J. Joachain, *Physics of Atoms and Molecules* (Longman, New York, 1983), pp. 207, 229.

[20] M. J. Goeckner and J. Goree, J. Vac. Sci. Technol. A **7**, 977 (1989).

[21] M. J. Goeckner, J. Goree, and T. E. Sheridan, in *Proceedings of the Fourth International Laser Science Conference, Atlanta, GA, 1988* (American Institute of Physics, New York, 1989), pp. 761–766.

[22] Michael G. Littman, Appl. Opt. **23**, 4465 (1984).

[23] S. Gerstenkorn and P. Luc, *Atlas de Spectre d'Absorption de la Molecule d'Iode*, (CNRS Editions, Paris, 1976).

[24] The ions can not be in thermal equilibrium in our discharge and as such, we use the term "effective temperature" rather than "temperature" to describe the ions. The ions cannot thermalize because the collision rate for ion–ion energy transfer is much less than the rate of ion loss. The formula used to calculate the ion–ion energy-transfer-collision rate can be found in David L. Book, *Physics Vade Mecum, 2nd ed.*, edited by Herbert L. Anderson (American Institute of Physics, New York, 1989), p. 280–281.

[25] M. J. Goeckner, J. Goree, and T. E. Sheridan, IEEE Trans. Plasma Sci. (submitted).

[26] Earl W. McDaniel, *Collision Phenomena in Ionized Gases* (Wiley, New York, 1964), p. 164.

[27] D. J. Koch and W. N. G. Hitchon, Phys. Fluids B **1**, 2239 (1989).

[28] W. R. Bennett, Jr., G. N. Mercer, P. J. Kindlmann, B. Wexler, and H. Hyman, Phys. Rev. Lett. **17**, 987 (1966).

[29] B. E. Cherrington, *Gaseous Electronics and Gas Lasers* (Pergamon, New York, 1979), p. 205.

[30] We have assumed that the cross section of this reaction is <1 Å^2. This is 10^4 times larger than the cross section of reaction (A4).

[31] W. T. Silfvast, D. Y. Al-Salameh, and O. R. Wood II, Phys. Rev. A **34**, 5164 (1986).